Three-dimensional Reconstruction of the Z Disk of Sectioned Bee Flight Muscle

Naiqian Cheng* and James F. Deatherage‡

*Department of Biology, Peking University, Beijing, People's Republic of China; and
‡Department of Biochemistry, University of Arizona, Tucson, Arizona 85721

Abstract. The three-dimensional structure of the central region of the Z disk of honeybee flight muscle has been determined to a resolution of 70 Å by three-dimensional reconstruction from electron micrographs of tilted thin sections. The reconstructions show a complex assembly in which actin filaments terminate and are cross-linked together; a number of structural domains of this network are resolved in quantitative three-dimensional detail. The central region of the Z disk contains two sets of overlapping actin filaments of opposite polarity, which originate in the sarcomeres adjacent to the Z disk, and connections between these filaments. The filaments are deflected by the attachment of cross-links; spacings between filaments change by >100 Å during their passage through the Z disk. Each actin filament is linked by connecting structures to four filaments of opposite polarity and two filaments are of the same polarity. Four types of connecting density domain are observed in association with pairs of filaments of opposite polarity: C1, C2, C3, and C5. Two of these, C3 and C5, are associated with the ends of actin filaments. Another connection, C4, is associated with three filaments of the same polarity; C4 is threefold symmetric.

THE Z disk is one of the basic structural units of striated muscle; it is a regular planar network of connections linking two sets of oppositely directed actin filaments from adjacent sarcomeres. A major component of the Z disk, the actin-binding protein α-actinin, is ubiquitous in structures of muscle and nonmuscle, actomyosin-dependent, cell motility. Three of the four domains of the Duchenne muscular dystrophy gene product, dystrophin, are homologous with the three domains of α-actinin; these homologous regions constitute all but 420 of the 3,685 amino acids of dystrophin (Koenig et al., 1988).

The Z disk of striated muscle is the most highly ordered representative of the largest class of cytoplasmic and membrane actin-organizing structures of muscle and nonmuscle cells. These structures contain α-actinin and are sites where actin filaments are cross-linked together and terminate. In addition to the Z disk, they include the intercalated disk of cardiac muscle, the zonula adherens of intestinal epithelium, the membrane and cytoplasmic dense bodies of smooth muscle, cytoplasmic stress fiber foci, membrane-adhesion plaques and junctions of cultured cells, and the cleavage furrow of mitotic cells (Tokuyasu et al., 1981; Geiger et al., 1981; Burridge, 1986; Lazarides, 1976). The membrane attachment structures of this class may play a role in the regulation of the motility and growth of normal and transformed cells (Buck and Horwitz, 1987; Burridge, 1986). The molecular linkages involved in the attachment and termination of actin filaments in these structures have not been determined. Among them only the Z disks of striated muscles exhibit regular structural repeats. The Z disk of insect flight muscle is especially highly ordered; we have used crystallographic electron image analysis of this Z disk to examine the structural details of a native complex of actin filaments and α-actinin.

Although Z disk specimens may be prepared for electron microscopy by negative staining or other procedures, the best ordered specimens available at present are thin sections of whole flight muscle. Perfectly transverse thin sections through the myofibril at the Z line are two-dimensional crystals; we have used crystallographic three-dimensional reconstruction from electron micrographs of tilted, transverse, thin sections (Amos et al., 1982) to image the arrangement of filaments and cross-linking structures in the Z disk.

Materials and Methods

Specimen Preparation

Freshly dissected honeybee dorsal longitudinal flight muscle was fixed in 2.5% glutaraldehyde in 0.1 M KCl, 0.01 M KPO_4, 0.001 M $MgCl_2$, 0.001 M EGTA, 0.001 M NaN_3 buffer for 3 h at 4°C, washed in two changes of buffer at 4°C, postfixed in osmium tetroxide (1%, 1 h at room temperature), dehydrated in ethanol, exchanged into *N*-butyl-glycidyl ether, and embedded in Quetol. The most reproducible results were obtained using freshly opened ampules of glutaraldehyde (Electron Microscopy Sciences, Fort Washington, PA; EM grade). The muscle is sensitive to distortion; careful handling was necessary to minimize mechanical stress on the fibers during dissection and fixation. Of the conditions investigated, those above gave the best preservation of fine detail and lattice order (six orders of image optical diffraction).

Table I A.

Series	Azimuth
1	0
2	0
3	89
4	89
5	149
6	149

B.

ID	Series	Angle	Compared	Error	Total
			n		*n*
14	1	00	36	2.4	36
16	1	+60	10	5.3	17
17	1	+55	15	7.6	23
18	1	+50	15	6.3	21
19	1	+45	18	7.8	23
20	1	+40	12	4.8	25
21	1	+30	16	6.1	30
22	1	+20	20	7.5	29
23	1	+10	16	5.4	34
25	1	−10	19	7.7	34
26	1	−20	21	7.7	29
27	1	−30	17	4.5	25
28	1	−40	16	6.6	23
29	1	−45	16	7.8	20
30	1	−50	16	4.1	22
31	1	−55	14	5.9	17
32	1	−60	11	6.0	15
33	2	−57.5	12	3.5	12
34	2	−52.5	13	4.2	15
35	2	−47.5	13	5.4	15
36	2	−42.5	20	5.2	21
37	2	−35	21	6.8	23
38	2	−25	26	3.9	26
39	2	−15	28	5.9	28
40	2	−05	36	5.6	39
43	2	+15	28	5.6	29
44	2	+25	27	5.6	29
45	2	+35	20	4.4	22
46	2	+42.5	23	5.7	27
47	2	+45	23	5.6	25
48	2	+47.5	25	4.6	27
49	2	+52.5	17	6.3	20
50	2	+57.5	17	5.7	19
52	3	−60	10	6.0	12
53	3	−55	13	7.8	17
54	3	−50	19	6.9	23
55	3	−45	22	7.9	28
56	3	−40	20	5.5	28
57	3	−30	25	8.4	38
58	3	−15	34	9.8	40
60	3	00	35	4.8	42
61	3	+15	34	4.4	43
62	3	+30	24	5.4	36
63	3	+40	19	7.1	26
64	3	+45	17	5.6	25
65	3	+50	19	5.2	26
66	3	+55	15	4.9	20
68	4	+52.5	15	6.0	15
69	4	+47.5	16	4.8	19
70	4	+45	14	7.3	14
71	4	+42.5	19	3.5	22
72	4	+35	21	5.5	22
73	4	+25	21	3.7	23
75	4	00	26	3.2	26
76	4	−25	23	7.2	23
77	4	−35	21	5.4	23
78	4	−42.5	18	5.5	19
79	4	−47.5	15	9.8	15
80	4	−52.5	12	5.0	12
81	4	−57.5	8	5.5	8
82	5	+60	8	7.4	11
83	5	+55	12	3.9	13
84	5	+50	11	3.0	12
85	5	+45	17	4.0	18
86	5	00	33	5.3	35
87	5	−45	19	4.9	20
88	5	−50	16	4.7	18
89	5	−55	15	6.0	16
90	5	−60	10	6.2	11
92	6	−52.5	17	3.8	19
93	6	−47.5	18	6.7	19
94	6	00	31	5.3	32
95	6	+47.5	15	4.2	17
96	6	+52.5	13	6.2	14

Statistics for three-dimensional reconstruction; merging of structure factors in P1. (*A*) (*Series*) Tilt series identifier. (*Azimuth*) Relative orientation of tilt axis for the tilt series. (*B*) (*ID*) Film number. (*Series*) Tilt series of film. (*Compared*) Number of structure factors from film compared in three-dimensional phase-origin refinement. (*Error*) Average merging phase error in degrees for film. (*Total*) Total number of structure factors measured for film.

Truly crystalline (i.e., perfectly transverse) thin sections are required for crystallographic image analysis by the usual methods (Amos et al., 1982). Gray thin sections (estimated to be ≤500 Å thick) were cut on a Sorvall Instruments (Newton, CT) MT-2 microtome; they were examined in the electron microscope to check orientation; the block orientation was successively corrected until the sectioning direction was perfectly transverse.

Electron Microscopy

Even a perfectly transverse thin section is unique in the location of its upper and lower surfaces relative to the myofibril axis. Because they are unique, it is necessary to collect full three-dimensional data sets of nearly 100 images from single Z disk specimens; data sets were collected in six tilt series about three tilt axes (Table I). To insure that the specimen did not shrink during the course of data collection, it was predosed until stabilized at the beam intensity used for photography, and then the images, each of 2-s exposure, were recorded using the controlled-dose procedure. Electron images were recorded on a JEOL USA (Cranford, NJ) 100CX-II electron microscope at 10,000×.

To monitor specimen stability, the three-dimensional structure factors of the specimen were evaluated as a function of cumulative electron dose. The six tilt series were designed to sweep sequentially through the data space so that the same regions of reciprocal space were sampled repeatedly at regular intervals over the course of data collection. The tilt series data were plotted on lattice-line plots with sequential exposure numbers indicated. The coincidence of the data points recorded in early and later tilt series indi-

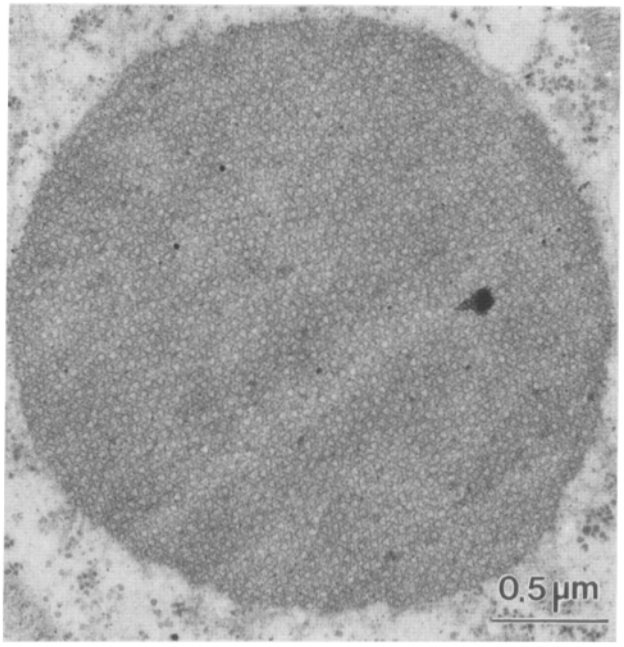

Figure 1. Transverse thin section through the Z disk of honeybee flight muscle.

cated that there was no change in the three-dimensional structure of the specimen over the course of data collection.

Selection of Data Sets

To select perfectly transverse views for crystallographic image analysis, computer-aided image enhancement was necessary; contrast on unprocessed images was too low to evaluate specimen orientation by eye. Several representative images at various angles of tilt were selected from the complete data set, digitized, and processed by computer. A local averaging procedure (Deatherage et al., 1989) was used to enhance contrast on the selected images; they were then compared on a common reference grid to locate perfectly transverse regions. Despite the prescreening of specimens, most of the three-dimensional data sets had to be discarded at this stage.

Image Processing

Images selected for processing were digitized on a Perkin-Elmer Corp. (Norwalk, CT) PDS microdensitometer on a 25-μm raster, corresponding to 25 Å on the specimen. Tilt parameters of the images were calculated by least squares refinement from the positions of gold marker particles, using the Align program (Lawrence, 1983; Luther et al., 1988). Before evaluating structure factors, precisely corresponding areas on the tilted views were masked out using vertices calculated from the tilt parameters. Preliminary lattice parameters for each image were calculated from the tilt parameters. Cyclic lattice refinement and evaluation and the selection of structure factors according to signal-to-noise ratio, figure of merit (Q), peak shape, and position were carried out by the pattern recognition program Autolat. Phase origins were refined in P1 (Amos et al., 1982). The merged data were sampled on a uniform lattice in z* using a convolution-smoothing procedure. Shaded surface representations of constant density surfaces of the three-dimensional maps (Radermacher and Frank, 1984) were computed for display using locally written software.

Results

One of the thin sections analyzed and its diffraction pattern are shown in Figs. 1 and 2. Since the thin sections are transverse, the myofibril axis, the optical axis of the microscope, and the z axis of the reconstructions are the same. Three three-dimensional reconstructions have been calculated. The data were collected in tilt series from −60° to +60° around three tilt axes at approximate relative orientations of 0°, 45°, and 90°; all lattice lines were densely sampled, up to the goniometer stage limit of 60° tilt. Statistically significant measurements of the amplitudes and phases of structure factors were made to a resolution of 70 Å along a number of lattice lines in three dimensions. Symmetry averaging of the three-dimensional structure factors after merging increased the effective sampling density by a further factor of three. The (1,k) row of lattice line plots of the three-dimensional structure factors before symmetry averaging are shown in Fig. 3; these plots are representative of the three-dimensional data. For the (1,4) lattice line only four structure factors were measured; this lattice line was omitted from Fig. 3. The data have <10° phase error for three-dimensional origin alignment (Fig. 3; Table I) and <12° phase error for P3 symmetry. The excellent phase agreement indicates a low error level for the three-dimensional map. The three reconstructions produced three-dimensional density maps which differed in their axial position but which were otherwise very similar.

Unprocessed micrographs and micrographs which had been subjected to varying degrees of local averaging by the procedure described in the accompanying paper (Deatherage et al., 1989), were examined to determine the projection symmetry. There was no evidence for a superlattice or for statistical disorder (for example, more than one pattern of unit cell contents occurring at random locations).

The primary mechanism of contrast formation in electron microscopy of thin sections is inelastic scattering of electrons by heavy metal positive stains bound to the component molecules of the specimen (proteins in the Z disk). The

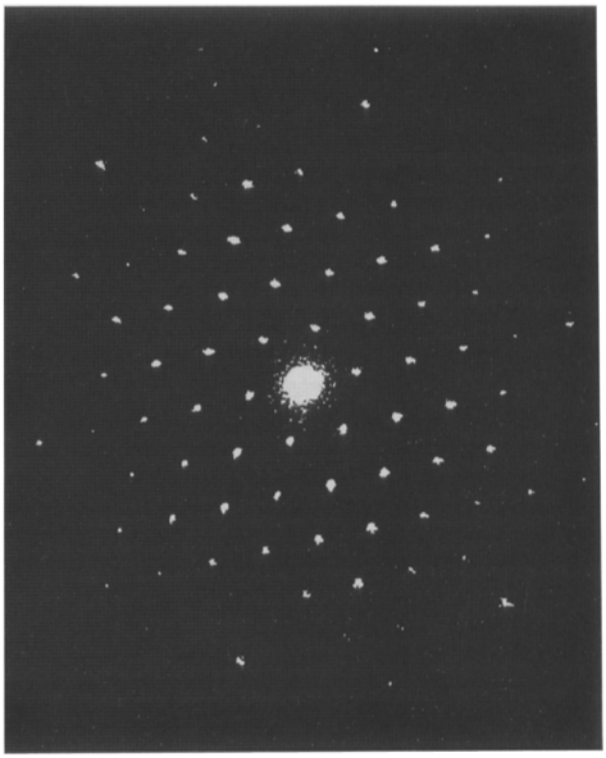

Figure 2. Optical diffraction pattern of the micrograph in Fig. 1.

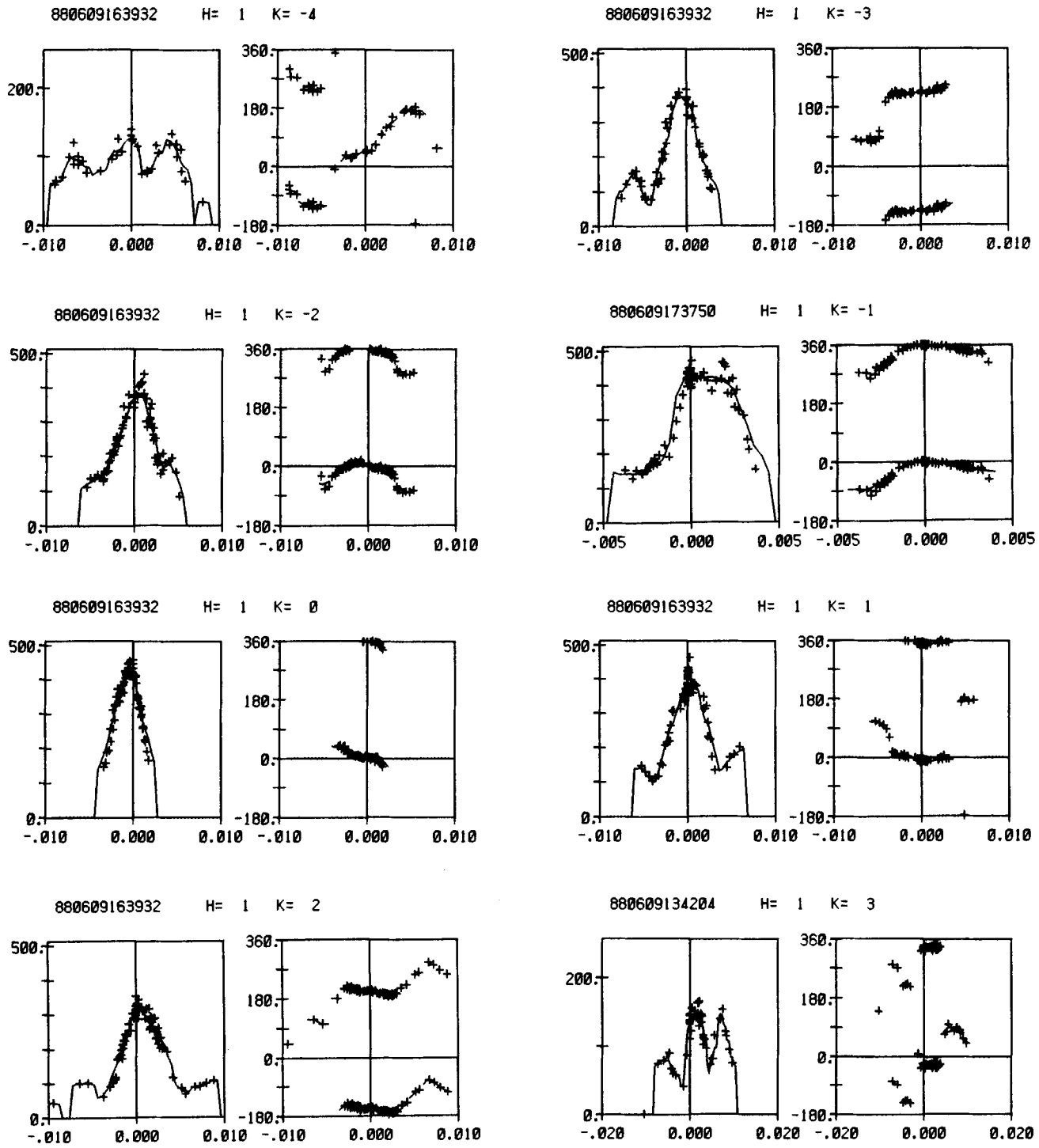

Figure 3. Plots of intensity (*left*) and phase (*right*) against z* in $Å^{-1}$ for experimental structure factors of the (1,k) lattice lines. The curves from which the uniformly sampled structure factors for three-dimensional reconstruction were sampled are shown.

three-dimensional structure analysis produces a three dimensional array of electron scattering densities, which are contoured at levels of constant density for display. These densities are related to the photographic densities of the data films by an arbitrary scale factor. The same density scale is used throughout the text and figures. The contours enclose regions of positive stain binding, which correspond to protein.

Our thin-sectioned muscle exhibited compression and shrinkage effects similar to those reported by Luther and Crowther (1984) and Luther et al. (1988) for fish muscle M line thin sections. As is usual, the thin sections were slightly compressed along the direction of sectioning. When compression effects are taken into account, the lattices on our images of honeybee myofibrils are hexagonal; the structure factors of Z disk images exhibit nearly perfect p3 symmetry. We concluded that the Z disk is organized on a hexagonal lattice and adjusted our images for compression by indexing the structure factors accordingly. The thin sections exhibit

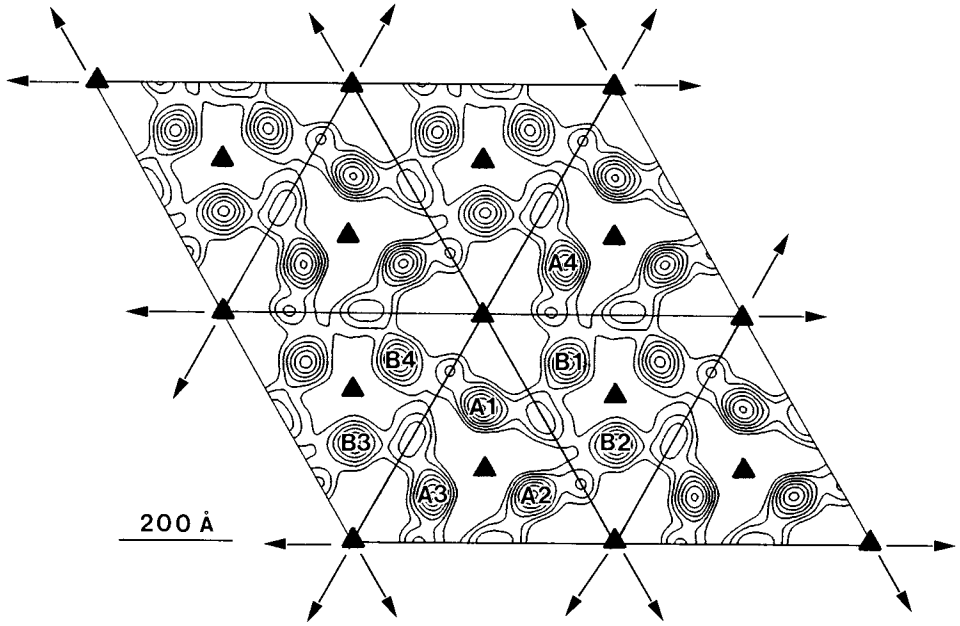

Figure 4. Key showing four unit cells of the central plane of the Z disk. The symmetry elements and numbering conventions for the filaments are indicated. Filaments are labeled A or B according to their sarcomere of origin.

shrinkage along their narrow dimension. The computed thickness of the density map was 200–250 Å, only about half of the thickness of the thin sections estimated from their interference colors. This is consistent with a shrinkage of 35–50% along the z axis (the narrow dimension perpendicular to the plane of the section); in their analysis of thin sections of fish M line Luther and Crowther (1984) observed the same degree of shrinkage. The exact scale along the z axis is uncertain; for presentation of the maps it has been expanded by a factor of two. The similarity of the three reconstructions calculated indicates that shrinkage along z is uniform, or at least reproducible.

Experimental Factors Affecting the Interpretation of the Density Maps

Several experimental factors affect the specimen features in the three-dimensional density maps produced by the structure analysis: limited resolution, missing data, and preservation and staining of specimen components. Because of these factors, the solvent protein boundary may not correspond to a single fixed density contour surface in the three-dimensional maps.

In this study we analyzed electron images crystallographically to measure periodic image components. The order of the crystal lattice is sufficient to produce statistically significant structure factors out to a resolution of 70 Å. The performance of the electron microscope is not limiting in this analysis. It records images to better resolution than the lattice order. In the (h,k,0) plane lattice lines ranged from 1/400 to 1/80 Å; data were measured out to 1/70 Å in three dimensions. The resolution of the analysis affects the reproduction of specimen features in the three-dimensional density maps. Low resolution reduces the detectability of smaller structures like slender filaments, since their density is spread out over a larger volume and may fall below the threshold for display.

The data for three-dimensional reconstruction of the specimen from views at varying degrees of tilt are incomplete. Views of the specimen at angles >60° off axis are inaccessible (the missing cone of data; Amos et al., 1982). The F(0,0,1) structure factors are a major component of the missing cone. The specimen contrast components arising from the F(0,0,1) terms (the axial or z density profile) can be observed as the integrated density variation with axial (z) position in images of longitudinal thin sections through the Z disk (side views). This variation was observed to be very small, indicating that the F(0,0,1) terms are small and the profile is relatively flat. Maps of locally averaged oblique sections (Deatherage et al., 1989) are in good agreement with the three-dimensional maps, providing a further check on the reconstructions.

Preservation and the intensity of staining of proteins in the specimen will affect their reproduction in the three-dimensional density maps. Some components may be disordered or extracted during fixation and staining. Features in the three-dimensional maps arising from well preserved and intensely stained specimen components would be expected to appear denser and larger on the maps. If specimen structures are partially disordered or extracted, or lightly stained, they may not be detectable. The integrated density of specimen features may not be directly proportional to molecular weight.

Overall Organization

The total thickness of the Z disk in the intact honeybee flight muscle is ~1,200 Å, comprising a central region of filament overlap >800 Å thick, and flanking regions several hundred Ångstroms thick. The central core of the Z disk stains well in conventional thin sections; its structure is the subject of this and the accompanying paper (Deatherage et al., 1989). There is also structure in the flanking regions on either side of the central core, but this is poorly stained in conventionally prepared thin sections.

The two-sided plane group of the whole Z disk is P312 (Deatherage et al., 1989). The threefold symmetry axes are

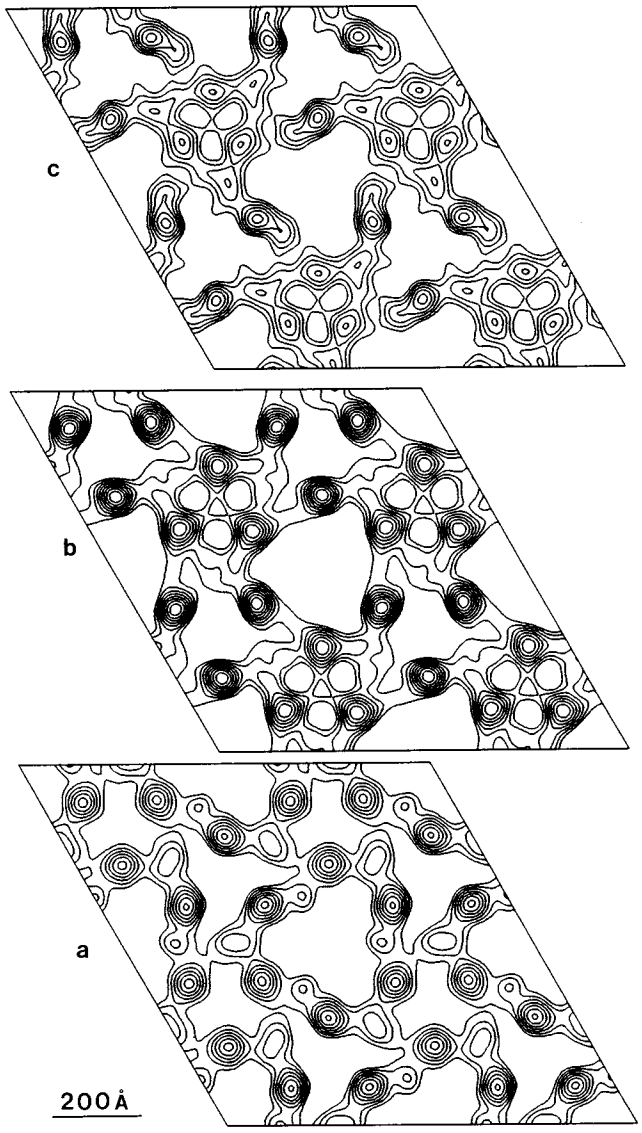

Figure 5. Planes through the three-dimensional density map. (*a*) Central plane. (*b*) Plane at the level of connection C4. (*c*) Plane at the level of connections C3 and C5. The contour interval is 1 on an arbitrary scale of density (see Results); the negative contour lines have been omitted.

parallel to the axis of the myofibril and perpendicular to the plane of the transverse thin sections and the three-dimensional density maps. The twofold axes of symmetry lie in the transverse central plane of the Z disk and are perpendicular to the myofibril axis. The thin sections from which the maps were calculated were cut near the center of the Z disk and include its central plane. The symmetry elements of the central plane are shown in Fig. 4. Planes of density through the three-dimensional density maps are shown in Fig. 5.

The minimum (solvent) density of the maps is −5.5, the maximum (protein) density is 7.9, and the average density is 0. The densest features (density >3) on the maps have been identified as extensions of the thin filaments by their positions in the lattice (Deatherage et al., 1989). The notation for their locations is shown in Fig. 4. The actin filaments appear as nearly uniform cylinders (Fig. 6); not enough helical variation in shape is observed to gauge reliably the azimuthal orientation of the filaments. Measurements of the diameter of the actin filaments depend on the density contour chosen. At the lowest density contour for which the filaments are separate features, their diameter is ~90 Å. The axial period of actin filaments is variable (Egelman et al., 1982) but, on average, an actin filament presents similar binding sites oriented at the same azimuth at ~375-Å axial intervals. The distance from the central plane to the end of actin filament overlap (~400 Å) corresponds to approximately one actin filament repeat.

Connecting density features are of lower density (<3) than the actin filament (>3.5). At the limited resolution of the analysis, this is expected for components which are smaller in diameter than the actin filaments and may consequently bind less stain. The resolution of these maps is not high enough to resolve internal structure inside the connecting features. More than one protein may be located in a connecting feature; alternatively, a single protein molecule may extend between different connecting features.

The thin sections include the central plane of the Z disk but are not centered on it. We refer to the sarcomere towards which the thin section is offset as the "B" sarcomere. We refer to the opposing sarcomere, located on the other side of the thin section, as the "A" sarcomere. The actin filaments from sarcomere B pass entirely through the reconstructed thin sections; the filaments from sarcomere A terminate part way through. Some structures of the Z disk nearer the A band of sarcomere B lie outside the thin sections and are not seen in our reconstructions.

Fig. 7, *a–d*, shows the three-dimensional density map. Like the original thin section, the map is a cross-sectional slab through the myofibril. Two constant density surfaces of the reconstruction are shown in Fig. 7; the semitransparent outer

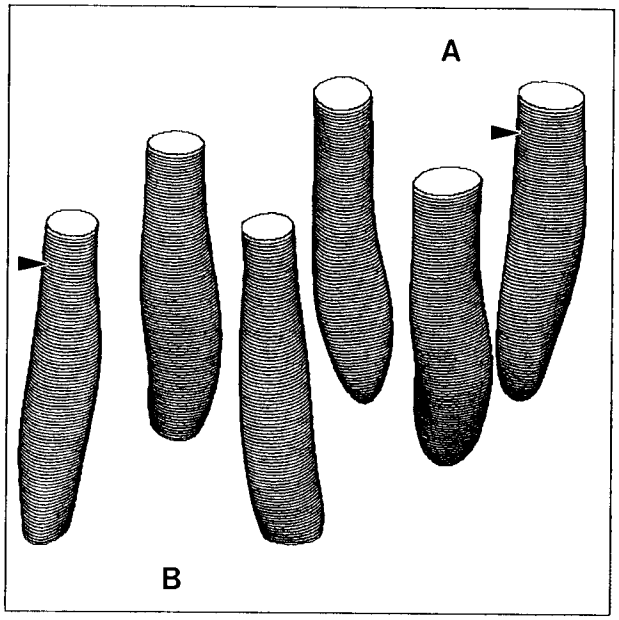

Figure 6. Contour surface of the three-dimensional density map at density level 3.5, which corresponds to the actin filaments. The direction of view is 60° off the myofibril axis. The sarcomeres of origin of the filaments are indicated. The approximate location of the central plane is marked with arrowheads.

surface corresponds to a density of 1.5 and the solid inner surface corresponds to a density of 3.5. The outer surface encloses densities of connecting features and actin filaments; the inner surface encloses densities of actin filaments. In Fig. 7 *a* sarcomere B and the viewer are above the map. The central plane of the Z disk is near the bottom of the map in this figure. In Fig. 7 *b* the map is viewed from the opposite side (sarcomere A and the viewer are above the map in this view). The central plane of the Z disk is near the top of the map in Fig. 7 *b*. Actin filaments from sarcomeres A and B and connecting density features C1–5 are labeled in Fig. 7. Because of the lower density of connecting feature C4, only its hub is seen (as a detached feature in Fig. 7 *a*).

Actin filaments from the opposing sarcomeres A and B overlap inside the Z disk. In Fig. 7 *a* it can be seen that the filaments entering the Z disk from sarcomere A (below the map) terminate partway up through the map. The filaments from sarcomere B pass all the way through the map. There are two ways to consider the grouping of filaments seen in Fig. 7: two polar groupings of three filaments originating in the same sarcomere (A or B), or one bipolar grouping of six filaments of alternating polarity. Fig. 6 is an approximately longitudinal view of a single unit cell of the lattice, showing the two different polar groupings of three filaments. The direction of view is ~60° off the myofibril axis; the constant density surface is at level 3.5. The group of three filaments on the right enters the Z disk from sarcomere A on the top of the figure; the group of filaments on the left enters from sarcomere B on the bottom. As groups of three filaments from the same sarcomere pass through the Z disk and approach the opposing sarcomere, they are deflected by the cross-linking network and move closer together. They also rotate as a group by ~11° around the axial threefold rotation axis which lies between them. The center-to-center distance between filaments in the polar groups of three is 230 Å in the A band, 215 Å where they enter the map, 170 Å at the central plane of the Z disk, and ~130 Å at their ends.

Fig. 8 shows a single lower constant density surface of the map (density level 0.5). As in Fig. 7, the slab is cross sectional, with its upper and lower surfaces transverse to the myofibril axis. The orientations of the top and bottom of the slab relative to the myofibril are the same as in Fig. 7. However, in Fig. 8 the slab has been rotated in its plane by 60° relative to its orientation in Fig. 7. The central plane of the Z disk is near the top surface of Fig. 8 *b*; the 32 symmetry of the central plane can be observed in this figure (only the threefold symmetry was enforced when the map was calculated).

The positions of the filaments originating in sarcomeres A and B are indicated. Although filaments from sarcomere A do not penetrate all the way to the top of Fig. 8 *a*, the positions of their ends in the lattice are marked on top with small circles or the letter A. Connection C4, a hub with three spokes, is located between three filaments from sarcomere A.

Connections between Actin Filaments

For purposes of description, the connecting density between the actin filaments of the map may be subdivided into five compact domains, C1–5. In this section we consider their relationship to the unit cell and its symmetry elements, to the actin filaments, and to each other. Four features are associated with filaments of opposite polarity (C1, C2, C3, and C5; Figs. 7 and 9), and one is associated with actin filaments of the same polarity (C4; Figs. 7 and 8). From the P312 symmetry of the Z disk, it can be deduced there are two sets of C3, C4, and C5 connections in the Z disk, one set on each side of the central plane. In the map only the sets near sarcomere B are observed. The other sets lie outside the section.

Connecting feature C1 is an axially elongated symmetric feature centered on a twofold axis in the central plane of the Z disk. In the transverse plane C1 lies closest to the filament pair A1–B1. The highest density for this connection lies to one side of these filaments, away from the threefold symmetry axis at special position 32 of the unit cell. Connecting density feature C3 is located above C1 in a similar position in the transverse lattice, but closer to sarcomere B. Connections C1 and C3 are continuous axially, but are partially separated by a constriction in the density between them. The continuous density can be seen in Fig. 9, *a* and *c*; the constriction can be seen in Fig. 9, *b* and *e*. The effects of the limited resolution and missing axial data on the analysis are to reduce contrast in the axial direction and blur together axially separated density features. We conclude that the constriction corresponds to at least a narrowing and possibly a gap between C1 and C3.

Like C1, connecting feature C2 lies on a twofold axis in the central plane of the Z disk. Its highest density lies closest to the filament pair A2–B2, but to one side of these filaments towards the threefold symmetry axis at special position 32 of the unit cell. C2 is illustrated in Fig. 9, where the C2 bridges between filament pairs A1–B4 or A4–B1 are shown. These pairs are equivalent by symmetry to A2–B2. Like C1, C2 is offset in position relative to the nearest pair of actin filaments, but its displacement is in the opposite direction. C2 is much smaller and less dense than C1. At lower contour densities it is somewhat axially elongated, although this does not show in the figures. At a contour density of zero, feature C1 from one grouping of six filaments and C2 from the adjacent grouping of six filaments are continuous along their common crystallographic twofold axis. It is possible that these structures are in contact, or that proteins common to both extend between them. Connecting density feature C5 is located above C2 in a similar position in the transverse lattice, but closer to sarcomere B (Fig. 9). The axial relationship between C2 and C5 resembles that between C1 and C3. However, the densities for C2 and C5 are better separated axially.

Connecting features C3 and C5 lie out of the central plane of the Z disk. C3 (B1→A2) is located between filaments B1 and A2 with a sidelobe connecting to filament A1. The distance between the centers of filaments B1 and A2 is ~240 Å. The full connectivity of C3 is shown in Figs. 7 *a* and 9, *a*, *d*, and *e*. A symmetry-equivalent C3 bridge (B3→A1) is shown in Fig. 9, *b* and *c*; in these figures the sidelobe (to A3) is cut off. C3 is located at or near the end of filament A2; density of feature C3 persists axially past the end of filament A2. C3 is situated in an asymmetric environment in the Z disk and has a polar, asymmetric shape. Feature C3 is near the top of the map and the part of C3 near filament A2 is less dense than the part near filament B1. If C3 is obliquely oriented, part of its A2 end may have been cut off by the knife during thin sectioning.

Only the part of connection C5 which is attached to the end

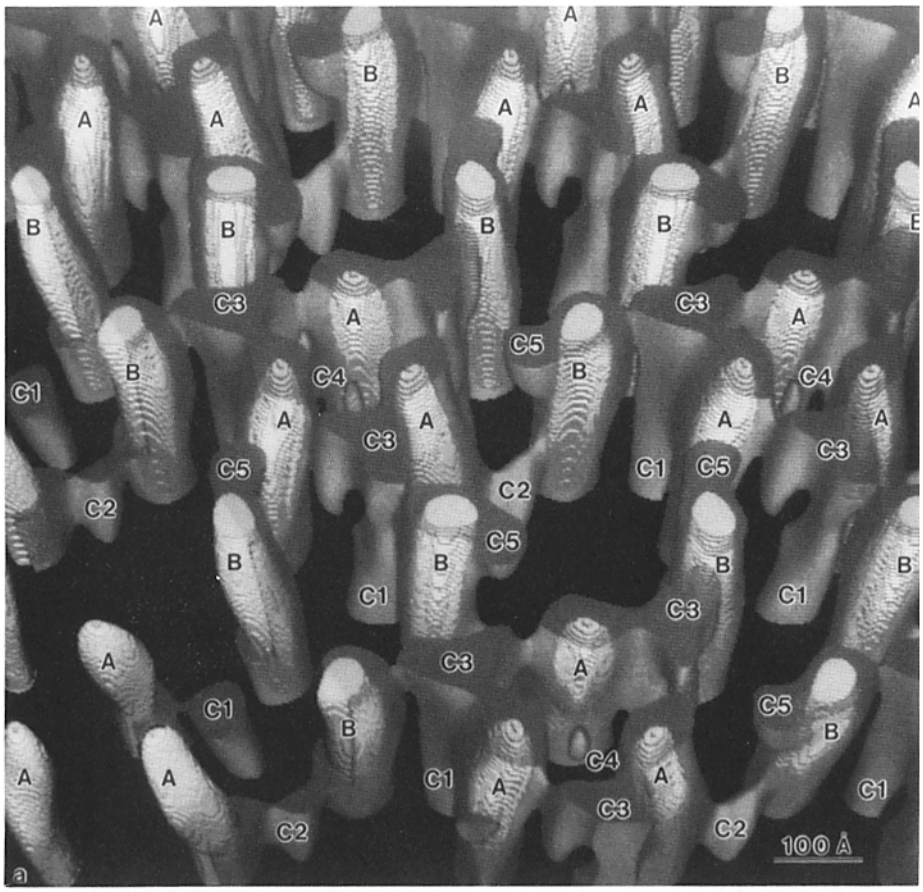

Figure 7. Shaded surface representation of the density level 1.5 (outer) and 3.5 (inner) surfaces of the three-dimensional map. The inner surface encloses the actin filaments. The outer surface encloses the cross-links. Filaments are labeled A or B according to their sarcomere of origin. Connections are labeled C. Features *C1* and *C2* are located at the level of the central plane. (*a* and *c*) View of the map from sarcomere B. (*b* and *d*) View of the map from sarcomere A.

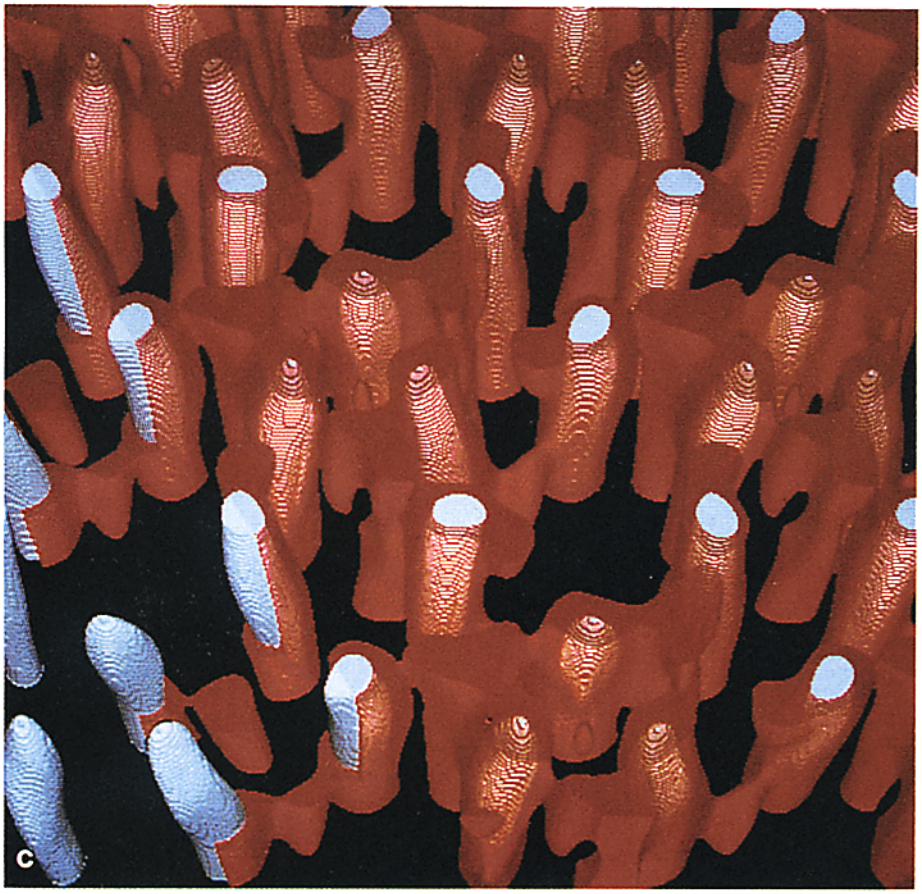
c

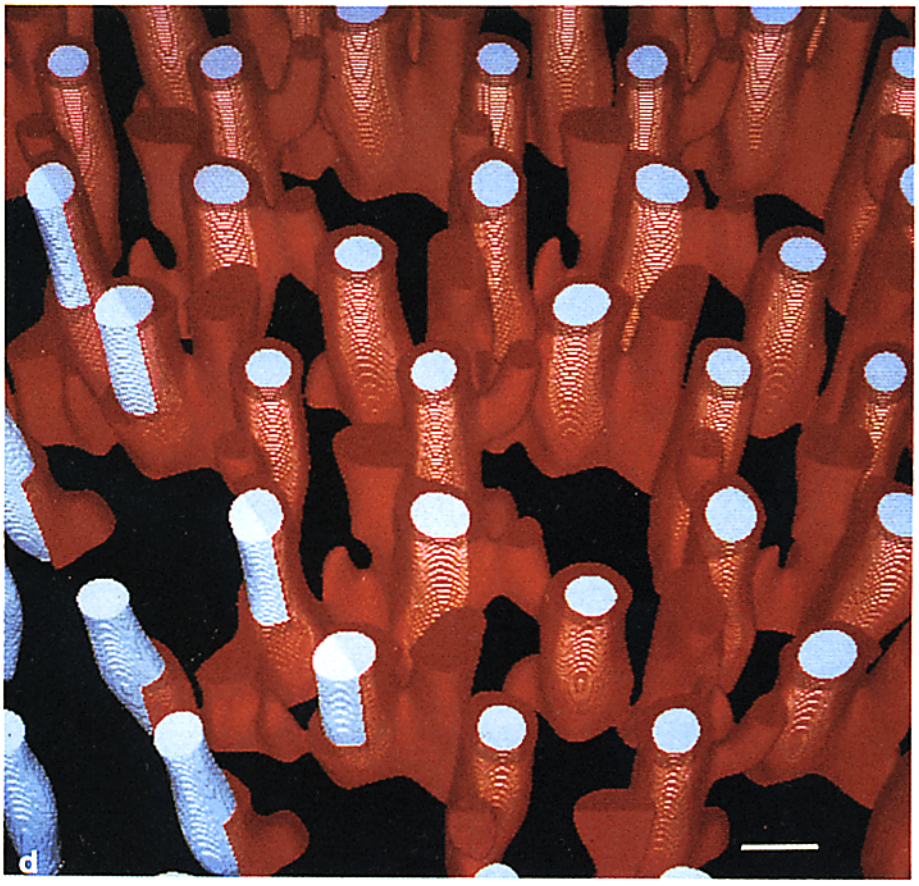
d

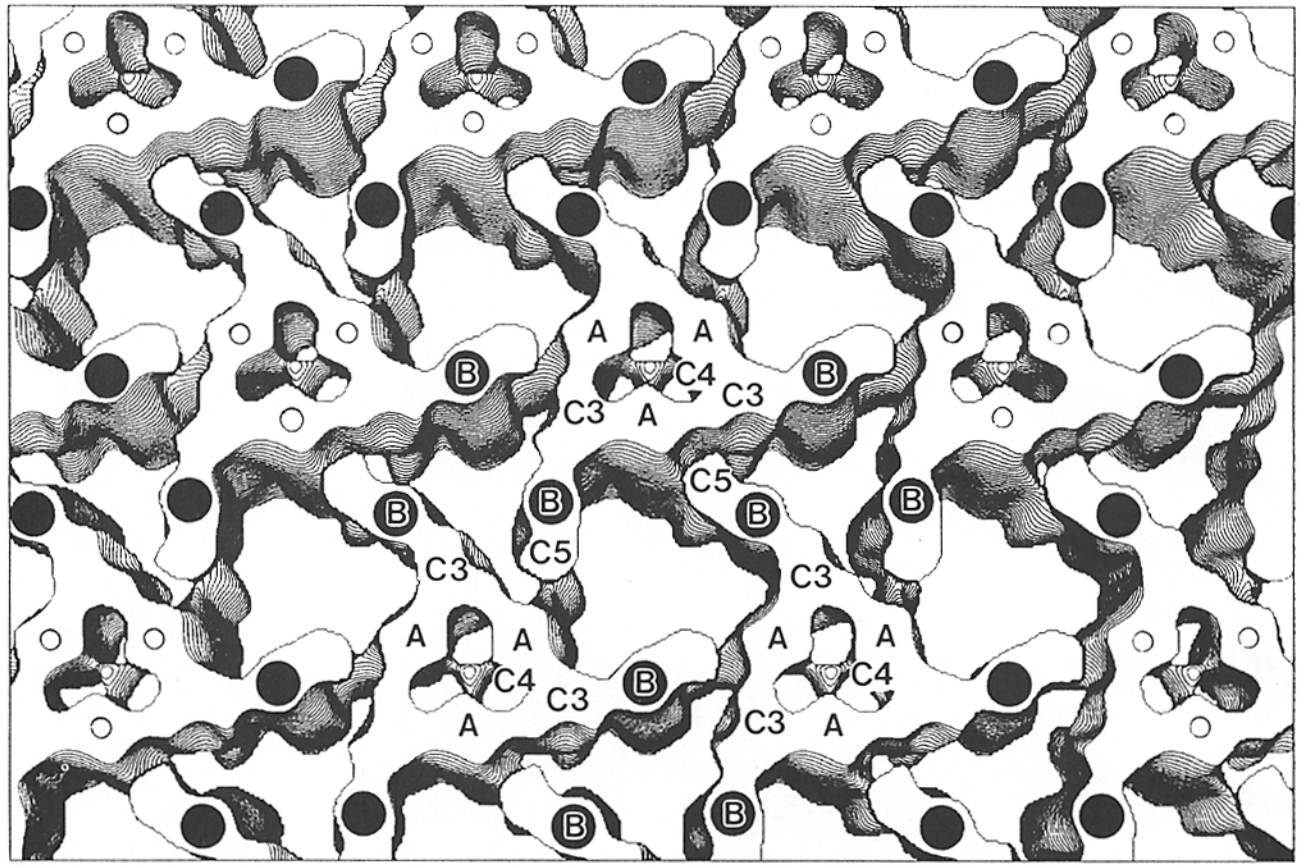
A
A
C4
C3
C3
A
B
B
B
C5
B
B
B
C5
C3
C3
A
A
A
A
C4
C4
C3
B
A
C3
A
B
B

a

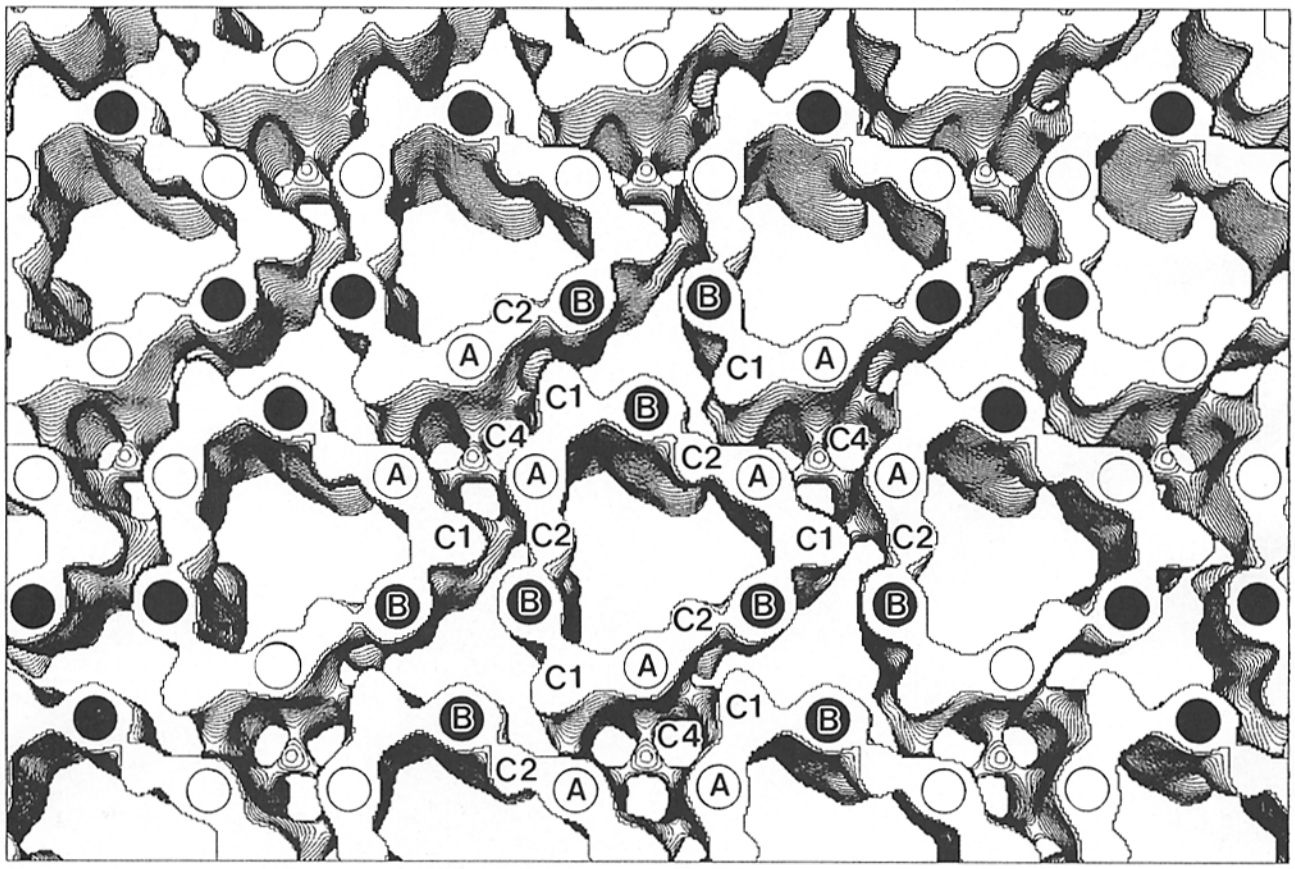
C2
B
B
A
C1
A
C1
B
C4
C4
C2
A
A
A
A
C1
C2
C1
C2
B
B
B
B
C2
C1
A
C1
B
C4
B
C2
A
A

b

200 Å

of the B filament is inside the map. However, this connection is observed on locally averaged, oblique, thin sections (Deatherage et al., 1989), allowing the connectivity (B2→A2) to be deduced. C5 is illustrated in Fig. 9, where the C5 connections on B1 (→A4) and B4 (→A1) are shown. These are equivalent by symmetry to the connection on B2 (→A1). The distance in the transverse plane from the end of filament A2 to filament B2 is 175 Å. The density for connection C5 persists axially past the end of filament A1.

Connecting feature C4 also lies out of the central plane of the Z disk. It is associated with three filaments of the same polarity from the same sarcomere (A1, A2, and A3). C4 has a lower density than C1, C2, and C3, but it is seen in all three reconstructions. It is shown at a contour level of 0.5 in Fig. 8; at a contour level of 1.5 only the central hub is seen (as a detached feature, Fig. 7 *a*). This connection differs in character from C1, C2, C3, and C5. It is threefold symmetric, consisting of three arms radiating from a hub on the threefold axis at the center of the three filaments. C4 is located near the ends of filaments A1, A2, and A3 on the side of the Z disk nearer to sarcomere B. The centers of the filaments like 80 Å from the threefold axis. The central hub of this threefold connection lies directly in line with the thick filament of the A-band of sarcomere B. If the connecting filament between that thick filament and the Z disk were extended directly into the Z disk it would intersect the hub of C4 (Deatherage et al., 1989). Although the hub is correctly positioned to serve as an anchoring point for the connecting filament, the reconstructions do not extend far enough to establish if a direct connection is made to the thick filament.

Discussion

The Z disk organizes, anchors, and terminates the thin filaments of the myofibril. It also anchors thick filaments and intermediate filaments (White and Thorson, 1973; Locker and Leet, 1972; Wang, 1982). Although the full role of the Z disk in the myofibrillar assembly and contraction is not known, the most prominent differences in structure between myofibrils in different types of striated muscle are in the Z disk. These differences presumably reflect differences in function.

The major component proteins of the Z disk are actin and α-actinin. In addition, a barbed-end, actin-capping protein isolated from muscle cells (a heterodimer consisting of subunits of 36 and 32 kD; Casella et al., 1986) has been localized to the Z line of skeletal muscle (Casella et al., 1987). This protein may be present in the Z disk of insect flight muscle as well. Other proteins of unknown function are also present (Sainsbury and Bullard, 1980). Some of the functions which may be mediated by different proteins are (*a*) cross-linking of actin filaments, (*b*) stabilization of the ends of actin filaments, (*c*) attachment of the thick filament to the Z disk, (*d*) attachment of transverse and longitudinal filamentous elements (for example, titin, nebulin, and intermediate filaments) to the Z disk, and (*e*) regulation of self-assembly into a bipolar, bounded structure.

Connecting Density Features

The connecting density features have been defined as approximately globular structural domains to simplify description of the map. However, this is not an absolute criterion for subdividing the densities. For example, C1 and part of C3 might have been designated as a single large axially elongated feature, and the remainder of C3 as a smaller adjacent feature. Nevertheless, five is the minimum number of domains which can describe the complexity of the structure. A single molecule may extend between two different features, in particular between C1 and C3, whose density is continuous axially, and possibly between C1 and C2, which are continuous at a much lower density level. Parts of more than one molecule may be located inside a single feature, especially inside C1, which is rather large and dense.

The connecting density features are located between (or adjacent to) the filaments specified in the Results section. It is most likely that the molecules in these features are attached to these nearby filaments. It is possible, but seems less likely to us, that they correspond to very elongated connecting molecules which are attached to other more distant filaments.

Features C1, C2, C3, and C5 are located in crystallographically and chemically nonequivalent environments in the unit cell. Examination of the map shows that the connecting features and their environments are quite different from each other. If these features are composed of several copies of a single type of protein molecule (for example, α-actinin), then these copies must exist in the structure in different conformations to adapt to their differing environments.

Relationship of α-Actinin and Connections C1, C2, C3, and C5

Actin and α-actinin are the major components of the Z disk. α-Actinin appears to be an integral part of most actin-containing structures in muscle and nonmuscle cells. α-Actinin of bee flight muscle has a molecular mass (SDS-PAGE) of 96 kD; chick smooth muscle α-actinin has 887 amino acid residues and a calculated molecular mass of 102 kD (Baron et al., 1987). There are three domains in the primary sequence of α-actinin: an NH_2-terminal actin binding domain (amino acids 1–240), a spectrin-like linker region (amino acids 270–740), and a COOH-terminal regulatory domain (amino acids 740–850). Sedimentation equilibrium and electron microscopy indicate that isolated α-actinin is a rod-shaped dimer 400 Å long and ~45 Å in diameter (Suzuki et al., 1976). The α-actinin dimer appears to contain two antiparallel monomers lying side by side in a bipolar complex

Figure 8. Contour surface of the three-dimensional map at density level 0.5. Filled circles indicate the positions of filaments originating in sarcomere B; open circles indicate the positions of filaments originating in sarcomere A. Connections are labeled C. Features C1 and C2 are located at the level of the central plane of the Z disk. (*a*) Map viewed from sarcomere B. In this view the positions of the filaments from sarcomere A, which do not penetrate all the way to the upper surface, are marked with small circles. (*b*) Map viewed from sarcomere A; in this view the central plane of the Z disk is near the top surface of the map.

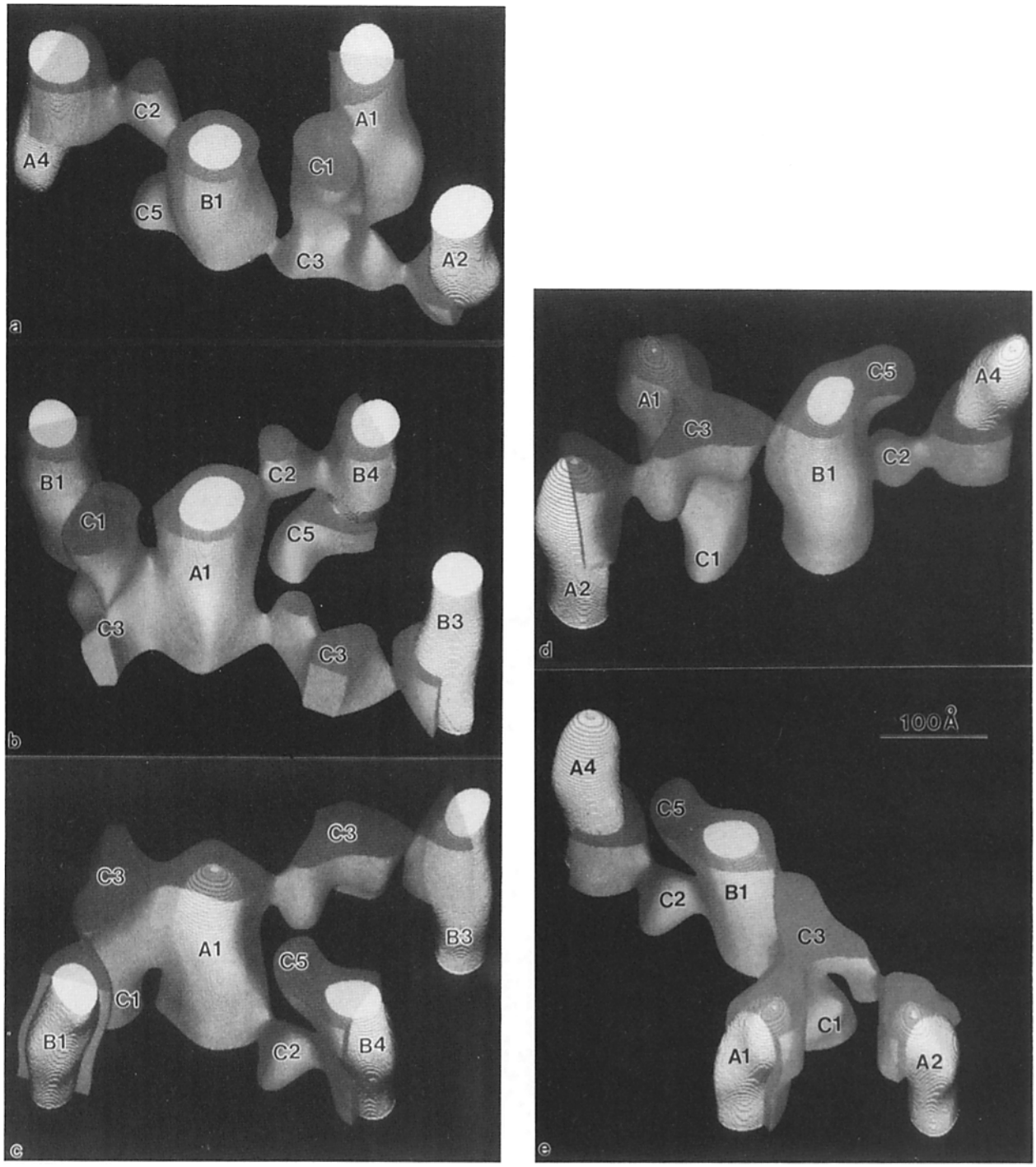

Figure 9. Details of the three-dimensional map. The density level of the outer surface is 1.5 and of the inner surface 3.5. Filament labels are the same as in Fig. 4. Connections are labeled C. (*a*, *d*, and *e*) Views of the connecting features surrounding filaments originating in sarcomere B. (*a*) Sarcomere A is up; (*d* and *e*) sarcomere B is up. (*b* and *c*) Views of the connecting features surrounding filaments originating in sarcomere A. (*b*) Sarcomere A is up; (*c*) sarcomere B is up.

(Wallraff et al., 1986). In complex with F-actin in vitro, α-actinin appears as the rungs in ladder-like structures in which the actin filaments are spaced ~350 Å apart (Podlubnaya et al., 1975; Jockusch and Isenberg, 1981), indicating that the actin binding sites are at opposite ends of the molecule. If we assume a maximum diameter of 90–100 Å for the actin filaments (Trinick et al., 1986; Egelman and Padron, 1984) then the central link region can be estimated to be ~250–300 Å long. The symmetry of α-actinin may be significant to self-assembly of the Z disk into a bipolar structure if its binding sites are oriented to link together antiparallel actin filaments.

The stereochemistry of the binding of α-actinin to actin filaments is poorly understood. It is unknown how many actin

monomers are involved in binding α-actinin, or at what spacings α-actinin molecules can bind to the same actin filament. It is also unknown whether the α-actinin dimer can bind proteins other than actin (for example, other α-actinin molecules or actin-capping proteins). The relative sizes of the binding and linker regions can only be roughly estimated. The conformational flexibility of the different domains of the molecule are unknown. All of these structural parameters are undoubtedly involved in determining the self-assembly and structure of the Z disk.

Relationship of α-Actinin to the Density Map

Since α-actinin is a major protein component of the Z disk, it is likely to be a major constituent of at least some of the observed connecting structures, in particular C1, C2, C3, and C5, which are associated with pairs of filaments of opposite polarity. Since no other components of the insect flight muscle Z disk have been characterized well enough, we can only consider how α-actinin might fit into the structure. This discussion is tentative because other proteins may be present in the network and contribute to the connecting densities.

The spacing of cross-linked filaments observed in the Z disk is closer (170–240 Å) than between actin filaments cross-linked by transversely oriented α-actinin molecules in vitro (~350 Å). These spacings may be accounted for by conformational flexibility of α-actinin, which may be able to assume a kinked or curved conformation, or by a partially axial orientation of the molecule. If we assume a simple model for α-actinin cross-links in which a linker of 250–300 Å spans the gap between filaments in an oblique orientation, we can estimate the binding geometry of cross-links built into the different features.

For a 250-Å link spanning the gap between filaments B1 and A2 through cross-link C3, the transverse distance spanned would be ~150 Å (240-Å center-to-center filament spacing minus filament radii), and the axial distance spanned ~200 Å. The connection to B1 may be closer to the central plane than the connection to A2, which may lie partially outside the map.

For a 250-Å link spanning the gap between filaments A2 and B2 through cross-link C5, the transverse distance spanned would be ~85 Å (175 Å minus filament radii), and the axial distance spanned 235 Å. The connection to B2 is closer to the central plane and would be located inside the map; the connection to A2 would be closer to sarcomere B and outside the map.

α-Actinin can be fit into features C1 and C2 in more than one way. In one interpretation of C1, a kinked link spanning from filament A1 through the center of feature C1 to filament B1, the transverse distance spanned would be 125 Å (215 Å minus filament radii) and the axial distance spanned ~225 Å. The binding site for one filament would be below the central plane and the binding site for the other above. A similar treatment of C2 gives transverse and axial spans of 90 and 235 Å. In an alternative interpretation of C1 and C2, one link connects filaments A1 and B2, and a second link, related to the first by rotation around the twofold axis in the central plane, connects B1 and A2. In this interpretation, for each link, part of the link is built into C1, and the remaining part is built into C2. For each link the minimum transverse distance spanned would be 150 Å (240-Å center-to-center filament distance minus filament radii) and the axial span 200 Å.

Varying the estimates of linker length and actin filament diameter does not affect the conclusion that oblique orientations must be assumed to fit the elongated α-actinin molecule into the connecting density features between the filaments. In some cases, the orientation of the link is predominately axial. All of the models described above, and other models not described, are consistent with the axial dimensions of the features observed on the maps. α-Actinin can be built into more than one model that fits the observed densities. It is interesting that feature C5, which can be modeled as a predominately axially oriented α-actinin molecule with a long axial span, was cut off by the knife during sectioning. Part of C3 may also have been cut off. This event would be more likely to occur in thin sectioning if the cross-link has a relatively long axial span.

Connection C4

Connection C4 has threefold symmetry. It consists of a central hub from which three arms radiate out to three actin filaments of the same polarity from sarcomere A. The hub of C4 occupies the position in the lattice which in the A band of sarcomere B is occupied by the thick filament. Thus, connection C4 is in the correct position to serve as an anchor for a C (connecting)-filament extending directly into the Z disk from the end of the thick filament of sarcomere B (Deatherage et al., 1989). However, the reconstructions do not extend far enough into sarcomere B to establish the presence of a continuous link. If the connecting filament is in a disordered conformation in unstretched muscle (see Ashhurst, 1977), stretching may be necessary to order it in the lattice so it will show up well in a crystallographic reconstruction. Further reconstructions of thin sections cut closer to the A band, perhaps using different staining conditions and stretched rigor muscle, are needed to provide structural evidence concerning the relationship of the connecting filament to C4. If it were indeed the anchoring site for the connecting filament, C4 would make an end-on connection between three actin filaments of one sarcomere to a thick filament of the opposite sarcomere.

Connection C4 differs in function and symmetry from the other connections. It cross-links filaments of the same polarity and has threefold symmetry. It is almost certainly composed of proteins different from those in the other connections.

Actin Filament Ends

Connecting features C1 and C2 are definitely associated with the sides of the actin filaments. The approximate locations of the ends of the filaments from sarcomere A can be estimated in the density maps. The connecting features have considerable axial extents. We estimate axial stratification as follows: start of thin section, central plane (upon which C1 and C2 are centered), constriction between C1 and C3, connection C4, end of density for filaments from sarcomere A, part of C5, end of thin section. Part of the density of C3 appears to be located beyond the axial level of the A filament ends. The density for C5 is axially beyond the level of the ends. The angles of attachment of C3 and C5 to the end of the filament of sarcomere A are only ~60° apart. C5 and possibly C3 may be connected to the terminal actins in the A filament, either on the side or capping the end of the fila-

ment. Connections C3 and C5 could account for stabilization of filament ends in the Z disk by sterically blocking addition of more actin subunits, and by stabilizing the terminal subunits in position by binding to them. If an actin-capping protein similar to the one located at the Z line in skeletal muscle (Casella et al., 1986, 1987) is present, it should be located at the junction of the end of the A filament with connections C3 and C5.

We thank Profs. Ray Nagel and Claire Payne (University of Arizona) for the use of their electron microscope, and Prof. Wah Chiu for the use of his film scanner. We thank Prof. Gu Xiaocheng of the Dept. of Biology, Peking University, for encouragement and support; Ms. Patricia Jansma for technical assistance; and Dr. Mike Schmid for comments. We also thank Prof. Gordon Waller and the staff of the U.S. Department of Agriculture Carl Hayden Bee Research Laboratory (Tucson, AZ) for their help with the bees.

This research was supported by National Institutes of Health Grant AM33141 and an American Heart Association (Arizona Affiliate) Grant-in-Aid to J. F. Deatherage.

Received for publication 28 December 1988.

References

Amos, L. A., R. Henderson, and P. N. T. Unwin. 1982. Three-dimensional structure determination by electron microscopy of two-dimensional crystals. *Prog. Biophys. Mol. Biol.* 39:183–231.

Ashhurst, D. E. 1977. The Z line: its structure and evidence for the presence of connecting filaments. *In* Insect Flight Muscle. R. T. Tregear, editor. North-Holland Publishing Co., Amsterdam. 57–73.

Baron, M. D., M. D. Davison, P. Jones, and D. R. Critchley. 1987. The sequence of chick α-actinin reveals homologies to spectrin and calmodulin. *J. Biol. Chem.* 262:17623–17629.

Buck, C. A., and A. F. Horwitz. 1987. Cell surface receptors for extracellular matrix molecules. *Annu. Rev. Cell Biol.* 3:179–205.

Burridge, K. 1986. Substrate adhesions in normal and transformed fibroblasts: organization and regulation of cytoskeletal, membrane and extracellular matrix components at focal contacts. *Cancer Rev.* 4:18–78.

Casella, J. F., S. W. Craig, D. J. Maack, and A. E. Brown. 1987. Cap $Z_{(36/32)}$, a barbed end actin-capping protein, is a component of the Z-line of skeletal muscle. *J. Cell Biol.* 105:371–379.

Casella, J. F., D. J. Maack, and S. Lin. 1986. Purification and initial characterization of a protein from skeletal muscle that caps the barbed ends of actin filaments. *J. Biol. Chem.* 261:10915–10921.

Deatherage, J. F., N. Cheng, and B. Bullard. 1989. Arrangement of filaments and cross-links in the bee flight muscle Z disk by image analysis of oblique thin sections. *J. Cell Biol.* 108:1775–1782.

Egelman, E. H., and R. Padron. 1984. X-ray diffraction evidence that actin is a 100Å filament. *Nature (Lond.).* 307:56–58.

Egelman, E. H., N. Francis, and D. J. DeRosier. 1982. F-actin is a helix with a random variable twist. *Nature (Lond.).* 298:131–135.

Geiger, B., A. H. Dutton, K. T. Tokuyasu, and S. J. Singer. 1981. Immunoelectron microscope studies of membrane-microfilament interactions: distributions of α-actinin, tropomyosin, and vinculin in intestinal epithelial brush border and chicken gizzard smooth muscle cells. *J. Cell Biol.* 91:614–628.

Jockusch, B. M., and G. Isenberg. 1981. Interaction of α-actinin and vinculin with actin: opposite effects on filament network formation. *Proc. Natl. Acad. Sci. USA.* 78:3005–3009.

Koenig, M., A. P. Monaco, and L. M. Kunkel. 1988. The complete sequence of dystrophin predicts a rod-shaped cytoskeletal protein. *Cell.* 53:219–228.

Lawrence, M. C. 1983. Alignment of images for three-dimensional reconstruction of non-periodic objects. *Electron Microsc. Soc. South. Afr. Proc.* 13: 19–20.

Lazarides, E. H. 1976. Actin, α-actinin, and tropomyosin interaction in the structural organization of actin filaments in nonmuscle cells. *J. Cell Biol.* 68:202–219.

Locker, R. H., and N. G. Leet. 1972. Histology of highly-stretched beef muscle. *J. Ultrastruct. Res.* 52:64–75.

Luther, P. K., and R. A. Crowther. 1984. Three-dimensional reconstruction from tilted sections of fish muscle M-band. *Nature (Lond.).* 307:566–568.

Luther, P. K., M. C. Lawrence, and R. A. Crowther. 1988. A method for monitoring the collapse of plastic sections as a function of electron dose. *Ultramicroscopy.* 24:7–18.

Podlubnaya, Z. A., L. A. Tskhovrebova, M. M. Zaalishvili, and G. A. Stefanenko. 1975. Electron microscopic study of α-actinin. *J. Mol. Biol.* 92: 357–359.

Radermacher, M., and J. Frank. 1984. Representation of three-dimensionally reconstructed objects in electron microscopy by surfaces of equal density. *J. Microsc. (Oxford).* 136:77–85.

Sainsbury, G. M., and B. Bullard. 1980. New proline-rich proteins in isolated insect Z-disks. *Biochem. J.* 191:333–339.

Suzuki, A., D. E. Goll, I. Singh, R. E. Allen, R. M. Robson, and M. H. Stromer. 1976. Some properties of purified skeletal muscle α-actinin. *J. Biol. Chem.* 251:6860–6870.

Tokuyasu, K. T., A. H. Dutton, B. Geiger, and S. J. Singer. 1981. Ultrastructure of chicken cardiac muscle as studied by double immunolabelling in electron microscopy. *Proc. Natl. Acad. Sci. USA.* 78:7619–7623.

Trinick, J., J. Cooper, J. Seymour, and E. H. Egelman. 1986. Cryo-electron microscopy and three-dimensional reconstruction of actin filaments. *J. Microsc. (Oxford).* 141:349–360.

Wallraff, E., M. Schleicher, M. Modersitzki, D. Rieger, G. Isenberg, and G. Gerisch. 1986. Selection of *Dictyostelium* mutants defective in cytoskeletal proteins: use of an antibody that binds to the ends of α-actinin rods. *EMBO (Eur. Mol. Biol. Organ.) J.* 5:61–67.

Wang, K. 1982. Myofilamentous and myofibrillar connections: role of titin, nebulin and intermediate filaments. *In* Muscle Development: Molecular and Cellular Control. M. L. Pearson and H. F. Epstein, editors. Cold Spring Harbor Laboratory, Cold Spring Harbor, NY. 439–452.

White, D. C. S., and J. Thorson. 1973. The kinetics of muscle contraction. *Prog. Biophys. Mol. Biol.* 27:173–255.